Journal of Crystal Growth 520 (2019) 96–104

Contents lists available at ScienceDirect

Journal of Crystal Growth

journal homepage: www.elsevier.com/locate/jcrysgro

Bubble distribution in fused quartz crucibles studied by micro X-Ray computational tomography. Comparing 2D and 3D analysis

Ove Paulsen[a,*], Stein Rørvik[b], Astrid M.F. Muggerud[c], Mari Juel[a]

[a] SINTEF Industry, Department of Sustainable Energy Technology, Trondheim, Norway
[b] SINTEF Industry, Department of Metal Production and Processing, Trondheim, Norway
[c] The Quartz Corp, Drag, Norway

ARTICLE INFO

Communicated by M.S. Goorsky

Keywords:
A1 Micro X-Ray computational tomography (μ-CT)
A2. Czochralski method
B1. Fused quartz crucible

ABSTRACT

Micro X-Ray computational tomography (μ-CT), has been applied to study the bubble distribution across the wall of fused quartz crucibles used for Czochralski pulling of monocrystalline silicon ingots for solar cells. Two crucibles from different suppliers has been used in the study. One set of samples was stored in water for 3 days ("wet" samples) and one set of samples was stored at 200 °C in air for 3 days ("dry" samples) prior to the first bubble analysis. Then the same samples were heated 24 h at 1400 °C and reanalysed. The μ-CT data were processed in 2D and 3D mode. The results showed that the total bubble volume was the same in 2D and 3D, while the number of bubbles was 6–9 times higher in 2D compared to 3D. The explanation was that in 2D each bubble was counted several times, while in 3D, each bubble was counted only one time. After heating the total bubble volume had increased to the double, while the number of bubbles was almost the same as in the unheated samples. There was no significant difference in bubble size or distribution between wet and dry treated samples.

1. Introduction

Gas bubbles in the inner wall of quartz crucibles for pulling single silicon crystals by the Czochralski (Cz) method can cause loss of structure of the Si-ingot when bubbles penetrate the inner wall and release gas or particles from the wall into the silicon melt. In the present work the bubble distribution across the wall thickness of two different crucible brands has been studied by micro X-ray computer tomography (μ-CT). The main purpose was to evaluate the μ-CT method as a tool to map the bubble distribution in the wall of quartz crucibles. μ-CT is capable to measure bubble size and bubble position in real 3D by scanning the sample cross section in "slices" of 9 μm thickness from the inner to the outer wall. By this method the position and size of every single bubble with diameter > 9 μm can be mapped. The samples need no specific preparation other than cutting and the sample size is typically in the range of a few cm^3 which is large enough to obtain excellent statistical data of the real bubble distribution in quartz crucibles. Since the method is non-destructive, the bubble distribution can be mapped on the same samples after different treatments. In the present work the samples were studied as received and after heated for 24 h at 1400 °C. Two parallel series were studied; one with samples kept 72 h in distilled water at 20 °C, denoted "wet" and one kept in a heat cabinet at 200 °C for 72 h, denoted "dry". The purpose with the wet treatment was to see if moisture exposure of the silica glass crucibles during storage could cause extra bubble formation near the surface during heating.

Quartz crucibles for Cz-pulling of mono crystal silicon ingots for solar cell production [1] are made of high purity quartz sand. The crucibles are manufactured by covering the inner surface of a graphite or steel mould with quartz powder and apply high power heating through electric arc discharge to melt the quartz sand [2]. A vacuum is applied on the outside of the mould to remove the air between the quartz grains during fusion of the inner layer of the crucible, to obtain a continuous movement of the melting front and to obtain an inner wall free from gas inclusions [3]. By turning off the vacuum after the innermost part of the wall has fused, a lot of air is entrapped in the outer part of the wall. The bubbles in the outer part serve to achieve a uniform heat transfer during crystal pulling compared to a bubble-free wall, and also give better mechanical stability. A fractured piece of a typical crucible wall is shown in Fig. 1. The almost bubble free inner layer of the wall and the outer layer consisting of a high density of bubbles are clearly visible.

Most of the commercial crucibles have wall thicknesses in the range 9–15 mm. The bottom is normally thicker than the vertical wall. Regarding gas bubbles, the inner 25–50% of the wall is normally almost

* Corresponding author.
E-mail address: Ove.Paulsen@sintef.no (O. Paulsen).

https://doi.org/10.1016/j.jcrysgro.2019.05.002
Received 15 August 2018; Received in revised form 16 April 2019; Accepted 6 May 2019
Available online 08 May 2019

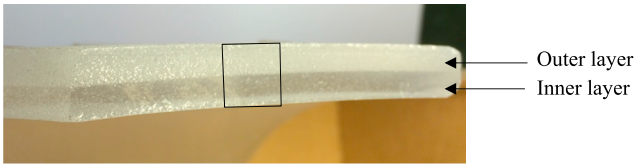

Fig. 1. A fractured piece of the vertical part of a typical Cz-crucible wall showing on top the outer bubble rich opaque part and below the inner almost bubble free transparent part. The square indicates how the samples were cut.

free from gas bubbles and is transparent. This is denoted the Bubble Free layer (BF). The outer 50–75% of the wall contains a lot of bubbles and is denoted the Bubble Containing layer (BC). The BC layer contains typically 0.5 vol% of gas inclusions and looks white translucent (see Fig. 1). The bubble concentration usually differs along the crucible wall as it can be very different in the bottom region compared to the vertical walls. The bubble diameter can be very large, a few hundred microns is not unusual. These bubbles are clearly visible to the naked eye. The crucible properties are defined by the quartz sand properties and the fusion process. The bubble distribution is dependent on the control of under-pressure during fusion of the crucible, and as the pressure control traditionally has been highly manual it is therefore natural that different suppliers will end up with a different bubble distribution.

During crystal pulling typically 1–2 mm of the inner wall is consumed because of reaction between Si and SiO_2 forming SiO gas: $Si + SiO_2(s) = 2SiO$ (g) [4,5,6]. Due to this, the innermost 1–3 mm of the crucible wall should be completely free from bubbles and no bubbles should be formed during crystal pulling. Bubbles that burst at the inner wall may cause defects in the silicon crystal that reduce the efficiency of the solar cell [7]. It is generally observed that used crucibles apparently contain more bubbles than un-used crucibles, and that the bubble size increases considerably during the crystal pulling cycle. During a typical Cz-pulling cycle the temperature is raised to 1500 °C in argon atmosphere at reduced pressure [8].

2. Experimental

Two fused quartz crucibles for Cz pulling were delivered from two different suppliers. The two crucibles are denoted A and B. The crucibles were examined in the as received state. By visual inspection Crucible A seemed to contain less bubbles than crucible B.

Samples were collected from the upper part of the crucibles approximately 80 mm from the top edge. From the original cuts that were approximately 50 mm × 50 mm × wall thickness (10–11 mm), two specimens with size 11–12 mm × 11–12 mm × wall thickness were cut from each crucible with a diamond cutting wheel (Fig. 2). The two samples were cut next to each other to have samples with as identical bubble distribution as possible before the experiments started. Since the μ-CT method is non-destructive, no further sample preparation was needed.

All specimens from each parallel were washed in ethanol in an ultrasound bath and dried. One specimen from each parallel was kept in a heat cabinet at 200 °C for 72 h. The other two were placed in glass bottles with distilled water and kept submerged in water at room temperature for 72 h. The two parallels of each crucible are denoted "dry" and "wet" respectively. After 72 h, the dry and wet samples were removed from the heat cabinet and water respectively. The bubble mapping was performed by using a Nikon XT H225ST NC Scanner, which enables a true 3D mapping of all bubbles by scanning the whole sample volume. Each scan covered cross sectional slices of thickness 9 μm. Each spatial pixel (voxel) was 9 × 9 × 9 μm^3. This means that bubbles with diameter less than 9 μm will not be detected. To cover each sample volume approx. 1200x1200x1200 voxels were needed. The bubble distribution and statistics were analysed by use of the computer program ImageJ [9] with the plug-in module 3D-OC [10]. The analysis was first done in 2D, mainly due to re-use of existing software methods and its much faster processing speed. The analysis was later redone in 3D, after establishing the required methods for cropping and segmenting the datasets in 2D. The analysed volumes in 3D was 6–13% larger than in 2D.

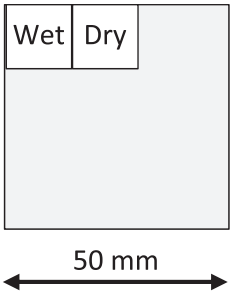

Fig. 2. The basic samples (large square) were ca. 50 × 50 mm^2 and cut from the upper part of the crucibles. The specimens subjected for bubble analysis were ca. 12 × 12 mm^2 and cut from the basic samples as shown above.

After measuring the bubble content in the original specimens, the specimens were heated to 1400 °C in air at ambient pressure and kept at 1400 °C for 24 h. The heating rate was 400 °C/h and the cooling rate 600 °C/h. After heat treatment, the bubble distribution was measured again. To keep control of the orientation in the CT-instrument one edge of each "cube" was cut oblique as demonstrated in Fig. 3. It shall be noted that the experimental heat cycle was not a simulation of a real Cz-pulling heat cycle which is performed at higher temperatures and lower pressure in inert atmosphere.

3. Results

3.1. Bubble volume – Wet and dry samples

The total measured bubble volumes and total analysed volumes are given in Table 1. In the table is also shown the corresponding calculated porosity (pore volume relative to analysed volume) and far right is the porosity measured by 2D relative to 3D calculated.

`The bubble volume versus bubble diameter for as received- and heat-treated samples A by 2D-and 3D analysis is shown in Figs. 4 and 5 respectively, and the corresponding analysis for sample B is shown in Figs. 6 and 7.

From Table 1 we see that the bubble volume of as received samples was typically 0.4–0.5 vol%. The 2D bubble volume is apparently higher than the corresponding 3D volume by a factor of 1.07 to 1.29. We also notice that "wet" and "dry" samples have practically the same volume fraction of bubbles before the heat treatment. For 2D analysis the difference (wet-dry/dry) is 2.9% for sample A and 8.5% for sample B. For 3D analysis the difference is 2.5% for sample A and −4.5% for sample B. This difference is within the variation measured between adjacent volumes of the same size which was estimated to ± 6%.

After heating to 1400 °C (red curves) we notice that the bubble volume has increased noticeably. From 3D analysis the increase for sample A was 76% and for sample B 95%, and the pore size distribution has shifted to larger pores. Before heating most of the bubble volume was due to bubbles in the range 30–70 μm. After heating this had shifted to 50–120 μm. The bubble size distribution in sample A is very similar to B, but for A the distribution is broader. Before heating 90% of the bubble volume was represented by bubbles with diameter less than 110 μm for sample A and less than 105 μm for sample B. After heat treatment the corresponding results were 135- and 120 μm.

3.2. Bubble distribution through the crucible wall

The pore volume distribution from the inner wall to the outer wall of the samples is shown in Figs. 8 and 9. The wall thickness has been divided in 4 equal sections, each representing 25% of the total wall

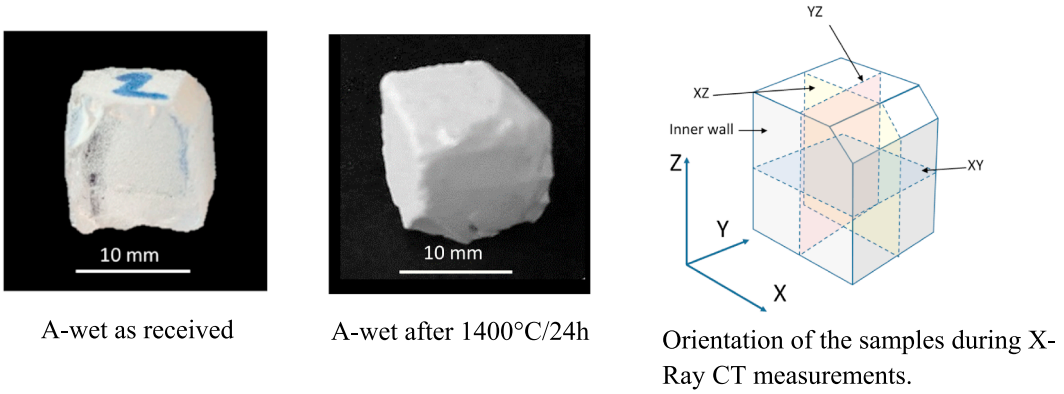

Fig. 3. Sample A-"wet" as received (left image) and after 24 h at 1400 °C (middle image). The sample orientation coordinates are shown far right. Notice that after heat treatment the surface was white and no longer transparent due to formation of cristobalite on the surface.

thickness, starting with section 1 at the inner wall. The bubble volume in each section has been calculated and the average values of wet and dry samples are plotted as points for each section. The measurements show little difference in bubble volume between 2D- (open symbols) and 3D analysis (filled symbols), in sections 1–3, but 2D analysis gave higher bubble volume at the inner and outer wall (section 4). We notice that most of the bubbles were located in section 3 in both crucibles. Heating to 1400 °C (solid lines), showed significant increase in bubble volume in sections 2 and 3 for sample A and less in section 1 and 4. For sample B significant increase was observed in section 1,2 and 3.

3.3. Number of bubbles

The average bubble concentration in the analysed volumes for wet and dry samples from 2D- and 3D analysis is shown in Table 2. We notice that the bubble number per mm^3 in average is 7.9 times higher in 2D compared to 3D. We also notice that the bubble concentration for wet and dry samples are very similar. For sample A as received, the pore concentration is the same for wet and dry samples. After heat treatment the pore concentration of the "wet" samples was 13% lower than for the dry samples.

2D analysis of sample B showed that wet samples had 2% higher pore concentration than the dry samples before heating and 9% higher porosity after heating. In 3D the corresponding pore concentration was 7% lower before heating and 1% lower after heating.

2D analysis indicates that the number of bubbles increased by 35% in average during heating to 1400 °C while in 3D the corresponding variation was 4%. The bubble number versus bubble diameter for the dry samples, are shown in Fig. 10 (sample A) and Fig. 11 (sample B). The dotted lines represent 2D analysis and the solid lines 3D analysis. The heat-treated samples are represented by red[1] coloured lines. We notice that for sample A, the 2D distribution (dotted lines) shows far more bubbles around 15 μm after heating than before. In 3D, the peak has moved to ca. 20 μm and the bubble number is less after heating than before. Looking at the bubble distribution for sample B (Fig. 11), we notice that the pore size distribution is very similar to sample A. In 2D there is a high peak at ca. 15 μm while in 3D the peak has moved to ca.

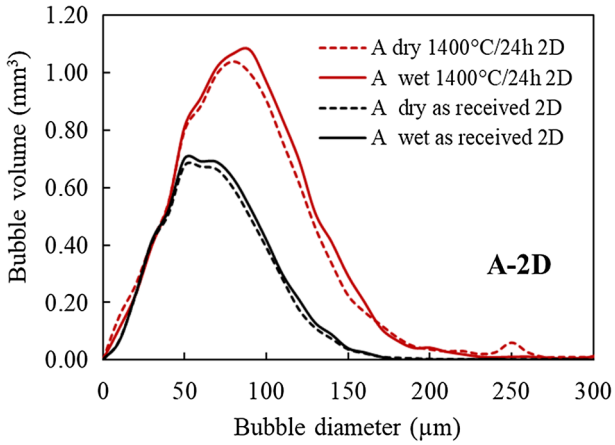

Fig. 4. 2D analysis of bubble volume versus bubble diameter for crucible A, wet and dry, as received and after heating 24 h at 1400 °C.

Table 1
Total analysed volume, total bubble volume and calculated porosity for 2D and 3D analysis of wet and dry samples as received and after heating 24 h at 1400 °C.

			An. sample volume		Total pore volume		Total porosity		Relative
Sample	Treatment		2D	3D	2D	3D	2D	3D	porosity
ID			(mm^3)	(mm^3)	(mm^3)	(mm^3)	%	%	2D/3D
A	As received	Wet	1207	1344	5.70	5.37	0.47	0.40	1.18
A	As received	Dry	1195	1347	5.48	5.25	0.46	0.39	1.18
A	1400 °C/24 h	Wet	1257	1423	10.63	9.33	0.85	0.66	1.29
A	1400 °C/24 h	Dry	1194	1312	10.15	9.59	0.85	0.73	1.16
B	As received	Wet	1224	1362	6.15	5.38	0.50	0.40	1.27
B	As received	Dry	1240	1370	5.75	5.67	0.46	0.41	1.12
B	1400 °C/24 h	Wet	1222	1296	11.75	10.38	0.96	0.80	1.20
B	1400 °C/24 h	Dry	1235	1312	10.60	10.51	0.86	0.80	1.07

[1] For interpretation of color in Fig. 10, the reader is referred to the web version of this article.

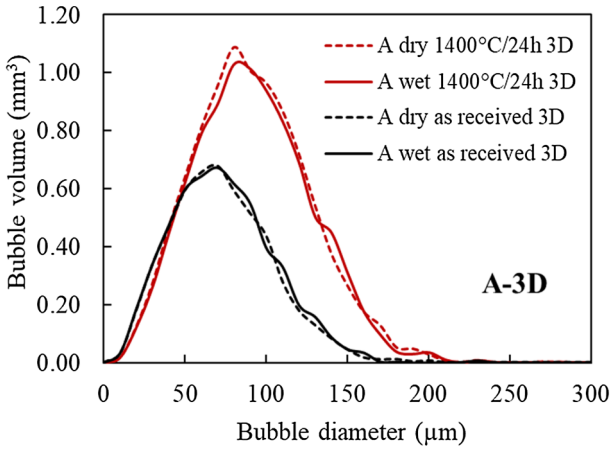

Fig. 5. 3D analysis of bubble volume versus bubble diameter for crucible A, wet and dry, as received and after heating 24 h at 1400 °C. After heating 24 h at 1400 °C.

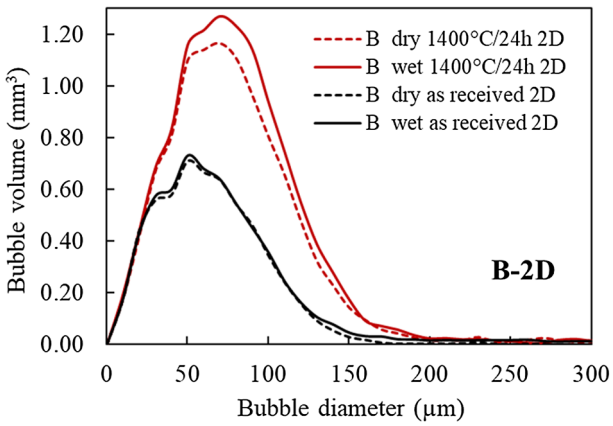

Fig. 6. 2D analysis of bubble volume versus bubble diameter for crucible B, wet and dry, as received and after heating 24 h at 1400 °C.

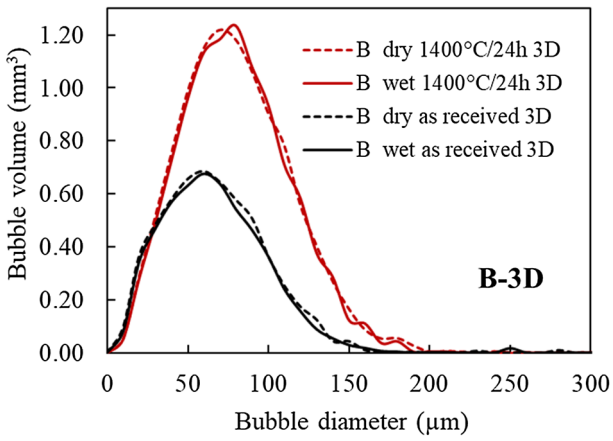

Fig. 7. 3D analysis of bubble volume versus bubble diameter for crucible B, wet and dry, as received and after heating 24 h at 1400 °C.

20 µm. The shape of the distribution curves is similar for as received and heat-treated samples.

3.4. Bubble distribution through the crucible wall

The mean number, (wet + dry)/2, of bubbles observed in the 4 sections of the crucible wall is given in Table 3. The same data are shown

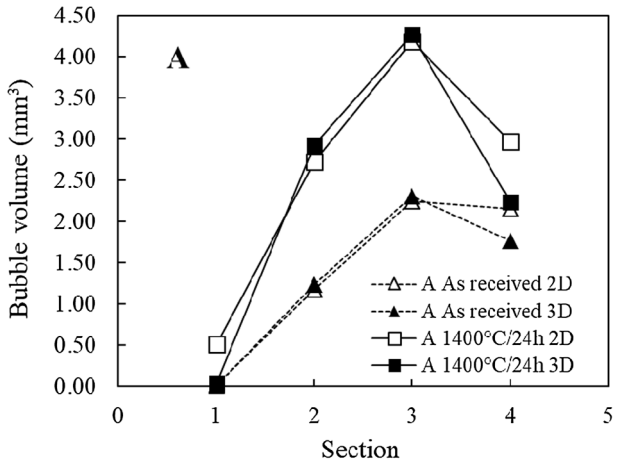

Fig. 8. Bubble volume distribution through the crucible wall for sample A. 2D and 3D analysis of as received and heat-treated samples.

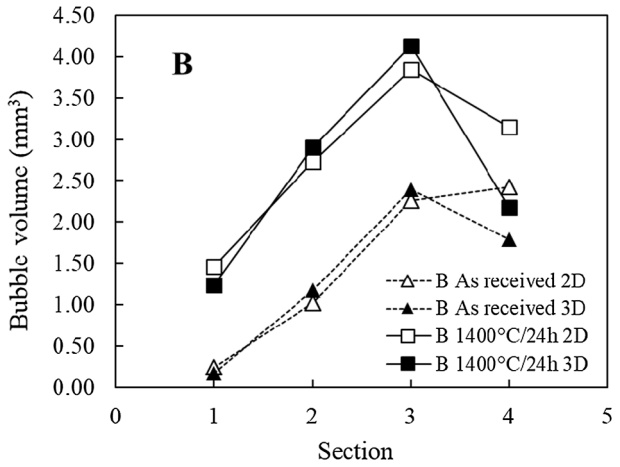

Fig. 9. Bubble volume distribution through the crucible wall for sample B. 2D and 3D analysis of as received and heat-treated samples.

Table 2
Mean pore concentration in the analysed volumes.

Sample	Treatment		Average pore conc. #·mm^{-3}		wet/dry	wet/dry
ID			2D	3D	2D	3D
A	As received	Wet	238	34	1.00	1.00
A	As received	Dry	239	34		
A	1400 °C/24 h	Wet	312	31	0.87	0.87
A	1400 °C/24 h	Dry	360	35		
B	As received	Wet	366	50	1.02	0.93
B	As received	Dry	357	54		
B	1400 °C/24 h	Wet	484	58	1.09	0.99
B	1400 °C/24 h	Dry	445	59		

graphically in Figs. 12 and 13. Comparing the total pore concentration (#·mm^{-3}) after heating compared to before heating, the concentration of bubbles in 2D-analysis, increased by a factor of 1.41 for sample A and 1.29 for sample B. The corresponding numbers for the 3D analysis were 0.97 and 1.12. The relative difference in bubble numbers between 2D and 3D analysis, showed that 2D analysis gave 6–9 times more bubbles than 3D. The distribution of bubbles through the wall shows that the number of bubbles were differently distributed in 2D compared to 3D. 2D analysis (Fig. 12) gave almost an constant increasing number of bubbles from the inner part (section 1) to the outer part (section 4), while 3D analysis showed a clear maximum in bubble number in section 3 (Fig. 13). The

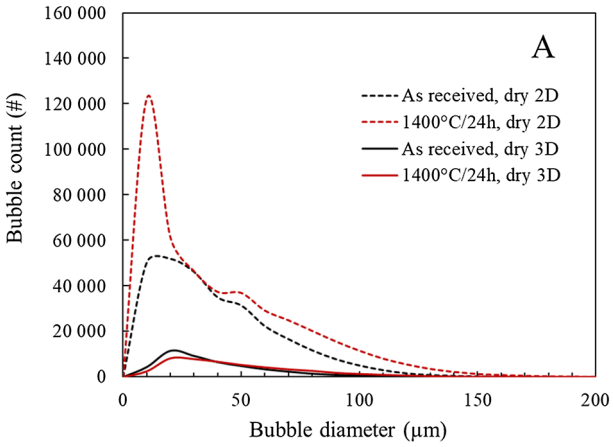

Fig. 10. Bubble number versus bubble diameter for Sample A, dry. 2D and 3D analysis compared.

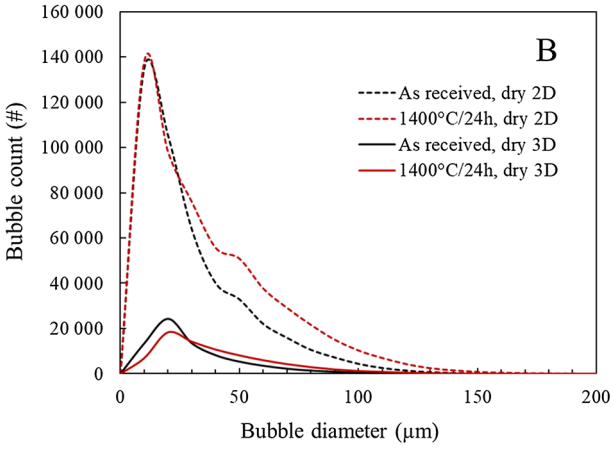

Fig. 11. Bubble number versus bubble diameter for sample B, dry. 2D and 3D analysis compared.

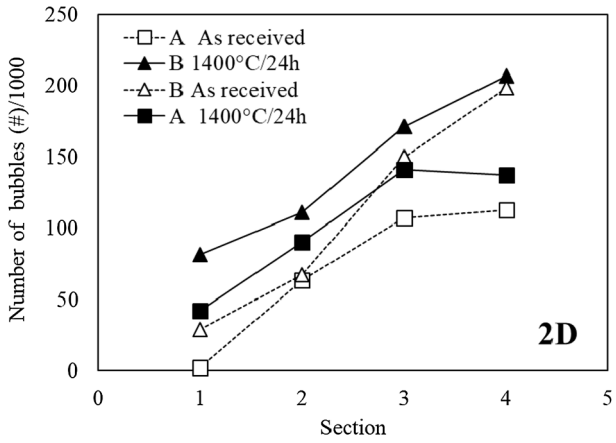

Fig. 12. 2D analysis of # bubbles, (wet + dry)/2, in each of four sections through the crucible wall of sample A and B, as received (dotted lines) and after heating 24 h at 1400 °C (solid lines).

3.5. Direct measurement of bubble growth

A direct measurement of changes in bubble size during heat-treatment was performed on a small volume (1.85 × 1.85 × 1.85) mm^3 from the centre of sample A. This volume contained ca. 300 bubbles. The size of every single one of these were measured before and after heat treatment. Fig. 16 illustrates the bubbles projected to the YZ plane before- (left image) and after heat-treatment (right image). A uniform increase in bubble size is seen. The overall bubble count has not changed significantly. Fig. 17 shows a 3D view of the same bubbles as shown in Fig. 16 before- (left), and after heat treatment (right).

The uniform increase in bubble size is easily visible. Some bubbles may appear to be missing in one of the images. This is because they are intersecting the edge of the analysed volume, and since the rotation of the datasets is slightly different (about one degree), the bubbles that intersect the edge will vary.

The intersected bubbles are removed by the analysis shown in

Table 3
Mean values, (wet + dry)/2, of bubble numbers pr. section through the crucible walls measured by 2D and 3D respectively.

Sample	Treatment	Dim.	*V*	Bubble count #·10^{-3} pr. section				Total
ID			(cm^3)	1	2	3	4	#·mm^{-3}
A	As received	2D	1.201	2.4	63.6	107.5	112.8	239
A	1400 °C/24 h	2D	1.225	42.0	90.1	141.0	137.6	335
B	As received	2D	1.232	29.0	67.6	149.9	198.6	361
B	1400 °C/24 h	2D	1.228	81.8	110.9	171.2	206.8	465
A	As received	3D	1.345	0.3	11.5	18.8	15.4	34
A	1400 °C/24 h	3D	1.367	0.9	11.8	18.8	13.6	33
B	As received	3D	1.366	5.2	13.2	29.8	23.2	52
B	1400 °C/24 h	3D	1.304	7.3	14.2	30.9	23.9	58

results show that sample A (square symbols) had a more even distribution of bubbles in section 2–4 compared to sample B (triangles).

3D analysis (Fig. 13) demonstrates clearly that the change in number of bubbles after heating compared to before heating was small. A more direct visual impression of the bubble distribution through the crucible wall is shown in Figs. 14 and 15. Here all bubbles in the analysed volume of "wet" samples A and B as received are depicted. The inner wall is at the left side. The Figures show that in sample A (Fig. 14) most of the bubbles were in the outer 2/3 of the wall while in sample B (Fig. 15), the bubbles were distributed in 3 distinct parts with increasing concentration from the inner wall to the outer wall. This is in line with the 3D analysis shown in Fig. 13.

Figs. 18 and 19

Fig. 18 shows a correlation of the 3D bubble volumes for the ~300 bubbles shown in Fig. 16. The dotted line is a simple linear regression of the data. The slope of the line is 2.02 indicating a doubling of the pore volume during heat-treatment. This relative increase is approximately the same for all bubbles, but some bubbles seem to have expanded more and some less. The slope represents an increase in pore diameter of 26.4%. Fig. 19 shows a correlation of the 3D bubble surface area for the ~300 bubbles shown in Fig. 16. The slope of the line in Fig. 19 is 1.69 corresponding to an increase in pore diameter of 30.0% regarding the pores as spherical.

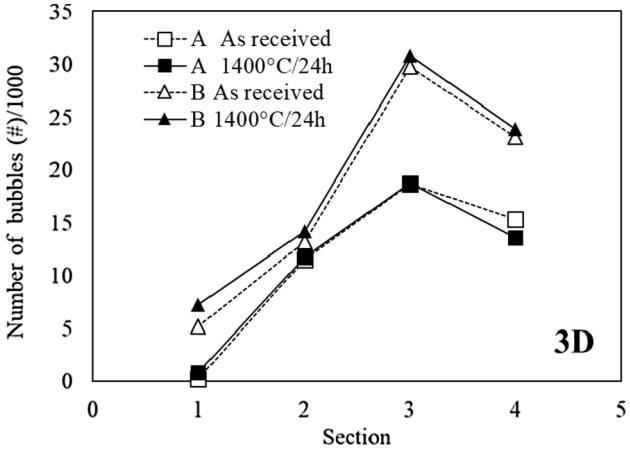

Fig. 13. 3D analysis of # bubbles, (wet + dry)/2, in each of four sections through the crucible wall of sample A and B, as received (dotted lines) and after heating 24 h at 1400 °C (solid lines).

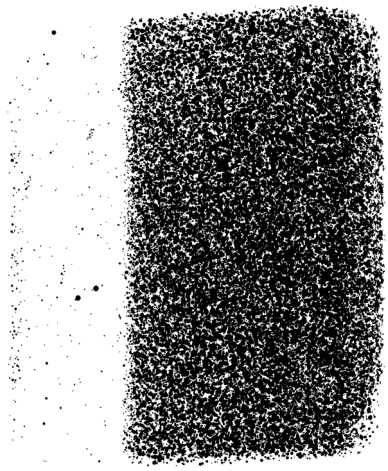

Fig. 14. Projection of all bubbles in the YZ-plane of sample A (wet) as received. Left side is the inner wall.

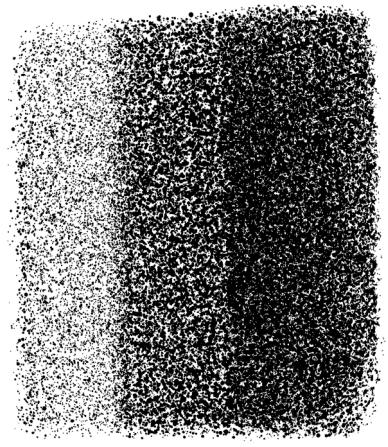

Fig. 15. Projection of all bubbles in the YZ-plane of sample B (wet) as received. Left side is the inner wall.

4. Discussion

4.1. Effect of water

The bubble size distributions of wet and dry samples before and after heating (Figs. 4, 5, 6 and 7) show that there was no noticeable effect of the water-treatment on the bubble size distributions. Since the wet and dry samples were different specimens cut from the same area of the crucible wall (see Fig. 2) a small difference in the bubble volume is expected due to statistical variations in the bubble distribution in the crucible. After heat treatment the bubble size distributions of wet and dry samples are still very similar except that the total bubble volume has increased. The observations support that the relative short exposure (3 days) to water at room temperature was not enough to cause excess bubble development during heating to 1400 °C. Diffusion of water into silica glass at low temperatures has been extensively studied by others [16,17,18,19]. Of direct relevance to the present work is the study of A. Zoudine et al. [16]. They measured the depth of water diffusion in silica glass submerged in water at 23 °C and $P = 2.8$ kPa in 9360 h (390 days). By measuring hydrogen profiles by a nuclear reaction analysis (NRA), the diffusion depth was estimated to 0.8 μm. Landford et al. [19] estimated the diffusion depth of water in silica glass to 100 Å in 2 months at 30 °C. If the diffusion is linear the estimated diffusion depth in 72 h should be ca. 0.006 μm. This implies that the water treatment of 72 h at room temperature should have no effect on the bubble formation during heating to 1400 °C. It is therefore reasonable to look at the wet and dry samples as two equal parallels. However, if hydrogen or water is present in the atmosphere during the crucible manufacturing process, water or hydrogen will enter the silica structure as OH^-. One water molecule will replace two oxygen bonds with two OH bonds and at the same time break one bond to adjacent Si atoms [11,12]:

$$\equiv Si - O - Si \equiv + H_2O \rightarrow \equiv Si - OH + OH - Si \equiv \quad (1)$$

By this, the glass structure becomes more open giving more space for the atoms to move, resulting in an increase in thermal expansion and reduction of the glass viscosity [20]. During heating the OH-groups can create sites for bubble formation and cause new bubbles to form. The reduced viscosity will cause the existing bubbles to grow faster than would be the case in a water free silica glass.

4.2. Bubble volume and size distribution

The visual impression of bubbles in crucible A and B as received was that crucible B contained more bubbles than A. This was confirmed by the bubble analysis shown in Table 2. In total, crucible B contained 51- and 53% more bubbles than crucible A before heat treatment by 2D- and 3D analysis respectively. The measured bubble size distribution for as received samples was practically the same in 2D and 3D with mean bubble diameters around 60 μm (Figs. 4 and 5). The average diameter of the bubbles can also be calculated from the average bubble volume (total bubble volume/total number of bubbles) in each sample, regarding all bubbles to be spheres. This has been done for sample A and B (wet + dry) in Table 4.

The results show that for sample A as received, the mean 3D bubble diameter is 60.4 μm, while the 2D diameter is 33.4 μm. After heating the average bubble diameter by 3D analysis was calculated to 73.7 μm for sample A and 64 μm for sample B representing an increase in diameter of 22% for sample A and 21% for sample B. The calculated 3D diameters are in line with the 3D bubble distribution in Fig. 5, while the 2D diameter is too low. This indicates that the number of bubbles in 2D analysis is far too high and that 3D analysis gives a correct number of bubbles. This can be explained by the measuring method. The instrument analysis the bubbles in slices of 9 μm thickness. This means that in 2D bubbles larger than 9 μm are counted more than 1 time. With an average bubble diameter of 60 μm each bubble will be counted 6–7 times. In 3D each bubble is counted only one time independent of the bubble size.

4.3. Bubble number

As mentioned above bubbles larger than 9 μm are counted more than one time in 2D analysis. When bubbles expand this will look as if

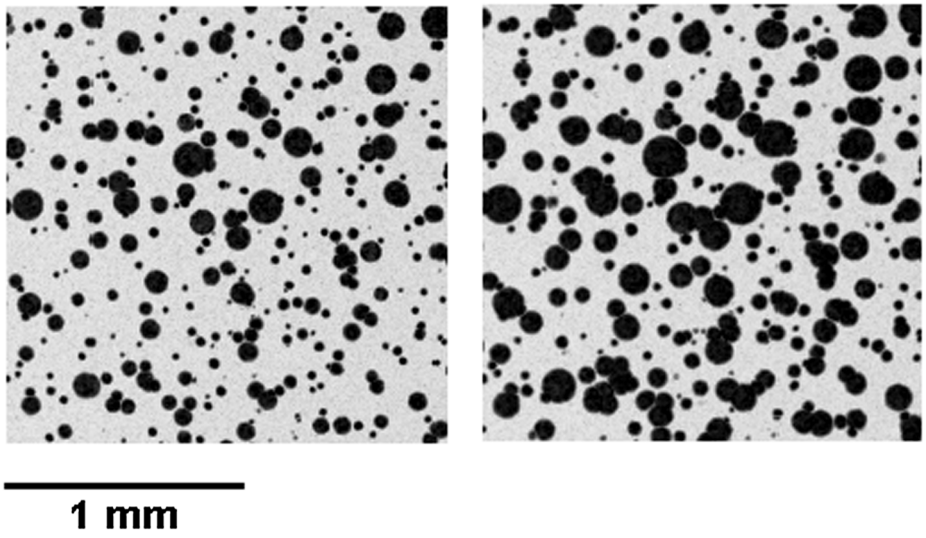

Fig. 16. Comparison of bubble sizes in sample A (dry) before (left) and after (right) heat treatment. Projection to YZ plane.

new bubbles are formed. As we have seen, 3D analysis gives the correct number of bubbles and reveals that the amount of bubbles is almost the same after heating as before heating. This tells that very few new bubbles were formed during heat-treatment of the crucible samples. The number- and distribution of bubbles are defined by the crucible manufacturing process. During reheating the number of bubbles may be reduced due to bubbles coalescing. This is observed. One factor that can increase the apparent number of bubbles is bubbles that are smaller than the detection limit before heating. If these expand to detectable sizes during heat treatment they will be regarded as new bubbles also in 3D analysis. That bubbles smaller than 9 µm exist in new quartz crucibles has been confirmed by Holand Hansen (2017) [15] who studied crucible samples in an optical microscope (resolution limit 1 µm).

Looking at the bubble volume we found that in 2D (Fig. 12), the samples apparently had higher bubble volume in section 1 and 4 compared to the corresponding 3D analysis (Fig. 13). The main reason for this is probably cracks formed close to the surface due to cristobalite formation. These cracks are not included in the 3D analysis because they are connected to the surrounding air volume, which is excluded from the analysis. In 2D large parts of these cracks appear as stand-alone-pores and are therefore included in the analysis results. The apparent increase in 2D bubble volume is therefore most pronounced at the outer crucible wall (Fig. 12).

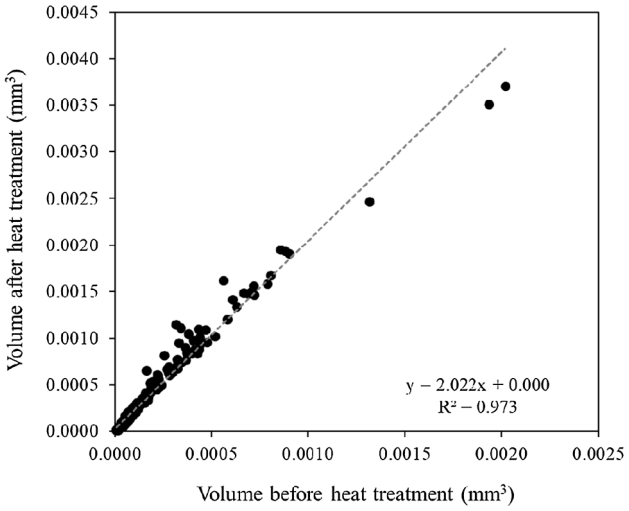

Fig. 18. Correlation of volume of the bubbles for sample A, shown in Fig. 16, before and after heat treatment.

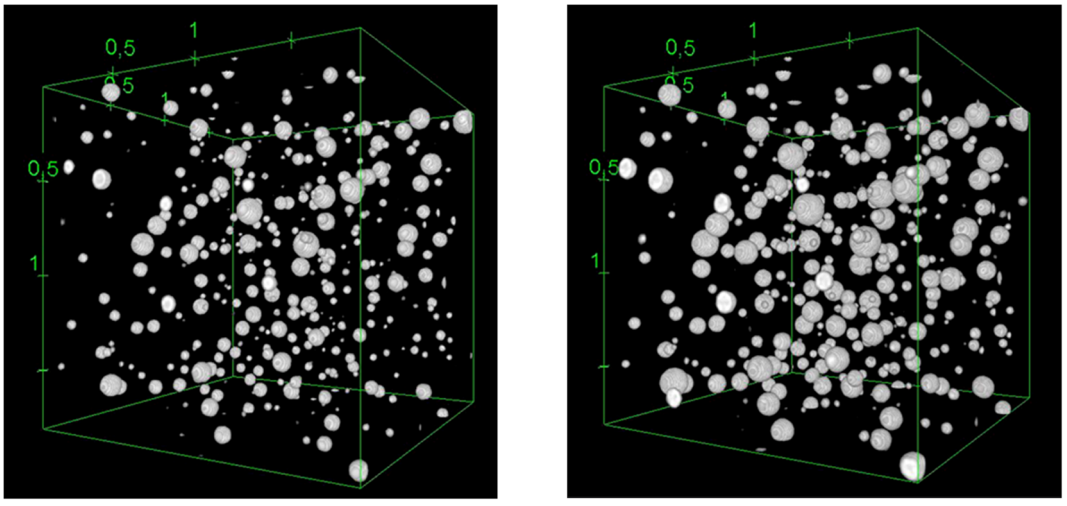

Fig. 17. 3D view of the bubbles shown in Fig. 16 (sample A) before (left) and after (right) heat treatment. Notice the increase in bubble size after heat treatment.

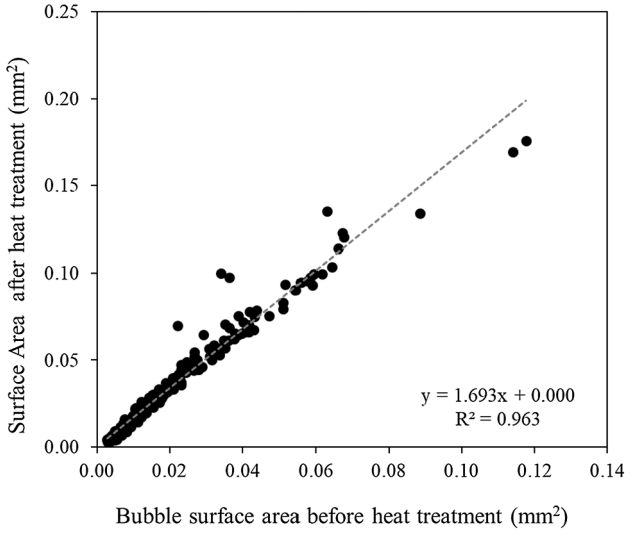

Fig. 19. Correlation of surface areas of the bubbles shown in Fig. 16 before and after heat treatment.

Table 4
Calculated average bubble diameter based on total bubble volume divided by number of bubbles.

Crucible	Treatment	Mean pore volume (mm^3)		Mean diameter (μm)	
ID		2D	3D	2D	3D
A	As received	1.952E-05	1.156E-04	33.4	60.4
A	1400 °C/24 h	2.317E-05	2.100E-04	36.4	73.7
B	As received	2.537E-05	7.744E-05	29.4	52.9
B	1400 °C/24 h	1.869E-05	1.370E-04	33.4	64.0

4.4. Bubble growth during heating

The direct measurement of bubble growth during heat-treatment of sample A (Figs. 18 and 19) showed that the volume increased by a factor 2.02, and the surface area by a factor of 1.69. If we look at the bubbles as spheres the volume is proportional to d^3 and the surface area is proportional to d^2. By using the volume expansion factor of 2.02 we find that this represent an increase in diameter of 26.4%. By using the expansion factor in surface area of 1.69 the diameter increase is calculated to 30.0%. This tells that the bubbles are very close to, but not perfect spherical shape. During expansion bubbles that coalesce will have geometries far from spherical shape.

By comparing the direct measurement of bubble expansion by the calculated mean expansion of the bubbles in sample A (Table 4), the calculated expansion was 22% which is 5%-points lower than the direct measurement. The direct measurement was performed on ≈300 bubbles in a volume of only 6.3 mm^3 while the data in Table 4 represent a volume of more than 1340 mm^3 and ≈460 000 bubbles. This large difference in the statistical basis might explain the difference between the direct and indirect estimation of bubble growth.

Since the crucibles are manufactured at temperatures above 1600 °C an increase in bubble size would not be expected by reheating to 1400 °C. Bubble growth during reheating of a crucible demands that gas has been transported from the bulk glass to the bubbles or that new gas species are formed inside the bubbles.

One gas source can be water (hydroxyl) in the glassy matrix that diffuses into the bubbles during reheating. This is supported by Z. Yongheng et al. (2006) [13] who demonstrated that water could be removed from silica glass by reheating at temperatures above 1200 °C. Another gas source is carbon particles in the bubbles [14] that reacts with SiO_2 forming different gas species (SiO, CO, CO_2, O_2) depending on the reaction mechanism. Xinming Huang et al. [20] analysed bubbles in fused silica before and after heating by using an optical microscope. Their sample was heated to 1500 °C for 10 h at 20 torr pressure. They identified three types of bubbles: H-type, N-type and A-type. The H-type was not visible before heating but expanded to very large bubbles during heating. These bubbles were related to carbon particles in the glass. During reheating carbon reacts with SiO_2 and can form SiO (g) and CO_2 gas by the reaction: $2SiO_2 + C = 2SiO + CO_2$. The N-type of bubbles was the “normal” type of bubbles. The expansion of these bubbles was proportional with the soak time at 1500 °C. The A-type bubbles were only observed close to the surface. These bubbles were more stable in size. The expansion mechanism suggested was that gas diffused from the bubbles to the argon atmosphere.

The gas composition in bubbles in new fused quartz crucibles and after they had been used for Cz pulling of silicon single crystals has been analysed using the "Time Of Flight Mass Spectrometry" (TOF-MS) method [22]. In new crucibles the analysed bubbles were from the bubble containing layer. In total 24 bubbles were analysed. In addition to gas composition also gas pressure at room temperature were measured. In used crucibles, 3 bubbles from the BF layer and three from the BC layer were analysed. The results are summarised in Table 5. The large scatter in the results can be explained by the small number of bubbles that were studied. The gas analysis shows that in the BC layer of new crucibles, three types of bubbles could be identified having different gas composition with respect to N_2, O_2 and CO_2. Type 1 had a gas composition close to natural air but had more CO_2 (1.4%). Type 2 and 3 had decreasing amount of oxygen and increasing content of N_2 and CO_2. The content of argon was ≈1% as in natural air. It is interesting to notice that neither hydrogen or water were detected in the bubbles. This might imply that water is not an important source for bubble formation and bubble growth. In the used crucibles we notice that the nitrogen level is less than 40 vol% and that the oxygen level is up to 77%. The argon level in the BC-layer is below 1% but in the BF layer, close to the silicon melt, the highest observed argon level was 11 vol%. As mentioned by Xinming et al. [20], carbon was observed in the large bubbles. Since manufacturing of fused quartz crucibles involves electric arch discharge heating by using graphite electrodes [21], carbon vapour or particles is to be expected in the atmosphere in addition to CO and CO_2. Carbon entrapped in bubbles might react with oxygen in the bubble to form CO_2. This will reduce the oxygen level and increase the CO_2 level in line with what is observed from the gas analysis of bubbles in new crucibles. However, the gas pressure will not change by this reaction. By reduction of SiO_2 by carbon the reaction

Table 5
Gas composition and gas pressure of bubbles in new and used fused quartz crucibles.

Crucible	Bubble	Layer	Bubbles	Gas composition in volume%				Pressure (mbar)	
	type		#	N_2	O_2	Ar	CO_2	RT	1400 °C
New	1	BC	7	81.5 ± 1.4	17.4 ± 1.0	0.82 ± 0.08	1.4 ± 1.4	364.3	2080
New	2	BC	8	83.6 ± 1.8	12.3 ± 1.2	0.96 ± 0.09	3.6 ± 1.8	525.1	2999
New	3	BC	9	85.7 ± 3.4	6.5 ± 2.4	0.87 ± 0.08	8.0 ± 2.4	328.0	1873
Used		BC	3	13–46	52–77	0.3–0.7	1.0–1.4	37.0	211
Used		BF	3	22–41	26–69	0.6–11.4	1.8–2.5	20.0	114

$2SiO_2 + 2C + O_2 = 2SiO + 2CO_2$ may take place. By this reaction carbon reacts with SiO_2 and oxygen forming SiO gas and CO_2 resulting in increased gas pressure. However, there are many possible reactions in the system SiO_2-C [24] and more work have to be done before the basic reason for bubble growth are fully understood.

In Table 5 the gas pressure inside the bubbles at 1400 °C has been calculated by using the ideal gas law and the measured gas pressure at RT. The result shows that at 1400 °C the pressure is 2–3 times higher than the normal atmospheric pressure. This represents a large driving force for bubble expansion during reheating. This alone can explain the bubble growth. However the reason for the excess pressure is so far not fully understood, and more research has to be performed to establish a full understanding of the reaction mechanisms.

In the Cz process the atmosphere is usually argon, and the process is run under low vacuum at ca. 1500 °C for several days depending on how many crystals that are produced from each crucible. The high content of oxygen and low content of nitrogen in the bubbles of the used crucible indicate that oxygen has diffused into the bubbles and nitrogen out. In contact with silicon the crucible dissolves and form O_2 by the reaction $SiO_2 = Si + O_2$ [23]. The high level of oxygen in the system close to the crucible wall might explain the high level of oxygen in the bubbles, but it also tells that gas diffusion through the glassy phase plays an important role regarding gas balance in the bubbles.

4.5. Effect of sample orientation

One error source is related to the sample orientation. Since the samples were removed from the μ-CT instrument between each heat treatment and the outermost surface was crackled, it was difficult to ensure that the samples were placed in exactly the same position each time. A small skew is enough to disturb the distribution function, while the total bubble volume and total number of bubbles is expected to be comparable since the whole sample volume was scanned in each analysis.

5. Summary and conclusions

The bubble distribution through the wall of samples from two different brands of quartz glass crucibles has been studied by X-ray μ-CT measurements. Two specimens of each crucible were examined. One kept 72 h in a heat cabinet at 200 °C (“dry”) and one kept submerged in distilled water for 72 h at room temperature (“wet”). Each sample was examined by μ-CT after dry and wet treatment (as received state), and after being heated 24 h at 1400 °C in air at ambient pressure. The aim of wet and dry treatment was to see if storage of crucibles in a humid environment influenced on the bubble growth and bubble formation, during the Cz crystal pulling process. The bubble distribution of each sample was analysed by 2D and 3D μ-CT calculations.

Comparing the 2D and 3D analysis showed that 3D analysis gave the most correct result with respect to number of bubbles and bubble volume. 2D analysis gave reasonably good estimates of bubble volume but 6–9 times too high number of bubbles. 3D analysis is therefore recommended.

The μ-CT measurements showed no significant difference in the bubble size distribution and spacial distribution between dry and wet treated samples, implying that storage of the crucibles at room temperature in humid conditions will not result in bad performance during crystal pulling.

During heating, the bubble volume measured by 3D increased by 70–90% in all samples. Direct measurement of bubble expansion of ca. 300 bubbles in sample A showed a volume expansion of 102%. Expansion of the bubbles during heating to 1400 °C would not be expected unless each bubble has been supplied by gas diffusing from the adjacent glass matrix into the bubbles or that gas forming reactions take place inside the bubbles. Analysis of the gas composition and gas pressure of bubbles in new fused quartz crucibles showed that all bubbles contained CO_2, but no sign of water. Bubbles with high CO_2 content showed low O_2 levels. This indicate that carbon particles in the furnace atmosphere play an important role in bubble expansion. It has been confirmed that carbon may be present inside the bubbles. Carbon can react with oxygen in the bubbles and form CO_2, but can also react with SiO_2 and form 2SiO(g) and CO_2(g). The latest reaction can give an overpressure in the bubbles and result in bubble expansion. Measurement of the gas pressure in bubbles at RT, showed that at 1400 °C the pressure would be 1–2 bar above ambient pressure. If this is real, this alone can explain the bubble expansion during heating to temperatures above the glass transition temperature.

The present work has shown that X-ray μCT-analysis is a powerful tool to obtain a true spacial distribution of bubbles in fused quartz crucibles. The method is not limited to glassy materials but can be applied to analyse pores and cracks inside any X-ray transparent material. Due to its non-destructive nature the method can be used to follow changes in the same selection of bubbles after different treatment of the sample.

Acknowledgements

This work was performed within” The Norwegian Research Centre for Solar Cell Technology” and sponsored by the Research Council of Norway and Norwegian research and industry partners. The μCT instrument was made accessible to our research group by The Norwegian Centre for X-ray Diffraction, Scattering and Imaging (RECX).

References

[1] L. Arnberg, et al., State-of-the art growth of silicon for PV applications, J. Cryst. Growth 360 (2012) 56–60.
[2] K. Kemmochi et al. US Patent 7,383,696 B2 (2008).
[3] M. Sakurada et al. US Patent 2010/0139549 A1.
[4] E.A. Guldbrandsen, et al., The high-temperature oxidation, reduction, and volatilization reactions of silicon and silicon carbide, Oxidation Metals 4 (1972) 181–201.
[5] X. Huang, et al., SiO Vapor Pressure in an SiO_2 Glass/Si Melt/SiO Gas equilibrium System, Jpn. J. Appl. Phys. 38 (1999) L1153–L1155.
[6] K. Abe, et al., Fused quartz dissolution rate in silicon melts: influence of boron addition, J. Cryst. Growth 186 (1998) 557–564.
[7] T. Minami, et al., In-situ observation of bubble formation at silicon melt-silica glass interface, J. Cryst. Growth 318 (2011) 196–199.
[8] Handbook of Silicon based MEMS materials and Technologies (2010). Chapter 2, Czochralski Growth of Silicon Crystals.
[9] C.A. Schneider, et al., NIH Image to ImageJ: 25 years of image analysis, Nature Methods 9 (2012) 671–675.
[10] S. Bolte, F.P. Cordelières, A guided tour into subcellular colocalization analysis in light microscopy, J Microsc 224 (3) (2006) 213–232, https://doi.org/10.1111/jmi.2006.224.issue-310.1111/j.1365-2818.2006.01706.x.
[11] A.K. Varshneya, Fundamentals of Inorganic Glasses. Soc. Glass Technol. (2006).
[12] V.N. Naraev, The influence of water on the glass properties, Glass Phys. Chem. 30 (2004) 367–389.
[13] Z. Yongheng, et al., The study of removing hydroxyl from silica glass, J. Non-Cryst. Solids 352 (2006) 4030–4033.
[14] X. Huang, et al., Expansion behaviour of bubbles in silica glass concerning czochralski (CZ) Si growth, Jpn. J. Appl. Phys. 38 (1999) L353–L355.
[15] S. Holand Hansen, Investigation of bubble distribution and evolution in solar cell quartz crucibles, Master Thesis, NTNU (2017).
[16] A. Zoudine et al. Diffusivity and solubility of water in silica glass in the temperature range 23-200°C.
[17] K.M. Davis, et al., Water diffusion into silica glass: structural changes in silica glass and their effect on water solubility and diffusivity, J. of Non-Cryst. Solids 185 (1995) 203–220.
[18] S.M. Wiederhorn, et al., Volume expansion caused by water penetration into silica glass, J. Am. Cer. Soc. 98 (2015) 78–87.
[19] W.A. Landford, et al., Diffusion of water in SiO_2 at low temperature. In Materials Science Research, Plenum Press, N.Y., London, 1985, pp. 203–208.
[20] H. Xinming, et al., Expansion of bubbles in silica glass concerning czochralski (CZ) Si growth, Jpn. J. Appl. Phys. 38 (1999) L353–L355.
[21] M. Fukui et al. Arch Discharge apparatus, apparatus and method for manufacturing vitreous silica glass crucible, and method for pulling up silicon single crystal. US. Patent US2010/0095881 A1 (2010).
[22] Private communication with Astrid M. F. Muggerud, The Quartz Corp (2019).
[23] K. Abe, et al., Initial dissolution of quartz rods in silicon melts: Influence of Quartz surface conditions, Jpn. J. Appl. Phys. 39 (2000) L644–L646.
[24] K. Wiik, Kinetics of reactions between silica and carbon. PhD- thesis. Institute of inorganic, Chemistry, University of Trondheim (NTNU), Norway, 1990.